Equilibrium Conformation of Concentric-Tube Robots Under Loads Based on the Minimum Energy Principle

Long Huang, Changyan He, Yang Yang and Chenhan Guang

Abstract Concentric-tube robots, which consist of several pre-curved tubes, can achieve dexterous motion through axial rotation and translation of each component tube. Aiming at equilibrium conformation modeling of externally loaded concentric-tube robots, an equivalent conservative system is proposed to translate the force balance problem into the minimum potential energy configuration problem of the conservative system. Then, the optimal control theory is used to derive the differential equations for the equilibrium conformation. Finally, this model is visually evaluated through the simulation of a loaded two-tube robot, and the effects of the external loads on the vital parameters of the equilibrium conformation are analyzed.

Keywords Concentric-tube continuum robots · Equilibrium conformation · Minimum potential energy principle · Kirchhoff rod

1 Introduction

Concentric-tube robots, as a special type of continuum robots, are well-suited for minimally invasive surgeries [1–3]. Normally, a concentric-tube robot consists of several concentric Nitinol tubes with different curvatures. Through axial rotation and translation of each tube, the shape of the tubes' common backbone can be

L. Huang · C. He · Y. Yang (✉) · C. Guang
School of Mechanical Engineering and Automation, Beihang University,
Xueyuan Road 37, Haidian District, Beijing 100191, China
e-mail: yang_mech@126.com

L. Huang
e-mail: huanglongmech@buaa.edu.cn

C. He
e-mail: changyanhe@126.com

C. Guang
e-mail: guangchenhan@foxmail.com

X. Zhang et al. (eds.), *Mechanism and Machine Science*,
Lecture Notes in Electrical Engineering 408,
DOI 10.1007/978-981-10-2875-5_18

altered, and consequently the pose of the robot's tip can vary within a certain range. Owing to the small diameter and simple structure, the concentric-tube robot can achieve dexterous motion under the narrow environment. Recent studies have already shown several potential clinic applications for these robots [4–7].

When the concentric-tube robot is used as a medical robot, a conventional task is to interact with the surrounding tissue. As a compliant mechanism, the robot will undergo a deformation during the interaction. Therefore, it is significant to study the precise equilibrium conformation of the robot subject to external loads. The general method adopted in prior researches is to analyze each tube with Newtonian mechanics and Kirchhoff rod theory, which is referred to as the geometrically exact model [8]. The processes of this method are as follows. First, the shape of each tube is described utilizing Kirchhoff rod theory; based on the linear constitutive equations, the relationship between moment and local curvature vector at arbitrary cross section for each tube need to be derived. Then, the force and moment balance equations for each tube are presented, and it is noteworthy that the unknown deformed shape of the tubes should be eliminated through the derivation of these equations. Furthermore, the equations about each tube's spin angle should also be deduced. Finally, by solving these equations, the equilibrium conformation can be obtained. The geometrically exact model is widely used to analyze both the concentric-tube robot and the cable-driven robot. Trivedi et al. [8] utilized geometrically exact Kirchhoff rod theory to model the shape of cable-driven robot under loads, and achieved high accuracy. Xu et al. [9] used four flexible rods instead of cables to build a small continuum robot, and they also used the geometrically exact model to derive the equilibrium conformation of the robot and furthermore achieve intrinsic force sensing. The models of these two cases are convenient to establish, since their components are under internal and external loads at discrete positions. However, the tubes in the concentric-tube robot are interacted continuously along the arc-length; therefore, the derivation of the geometrically exact model for the concentric-tube robot is more complicated [10, 11].

In order to avoid the complex interaction analysis of the tubes, this paper proposes an equivalent method which transform the force balance problem into the equilibrium problem of the conservative system. Then, applying the minimum potential energy principle of conservative system and the optimal control theory, the differential equations which describe the equilibrium conformation can be acquired. For clarity in deriving the equations, this paper focus on the shape modeling of the three-tube robot subject to concentrated forces at its tip, and the proposed method can also be used in the robot with arbitrary number of tubes subject to distributed forces and torques.

2 Description of the Concentric-Tube Robot

A concentric-tube robot usually comprises two or three Nitinol tubes, and achieves 3–6 degrees of freedom. These elastic tubes are assembled concentrically. Through axial rotation and translation of each component tube, the shape of the tubes' common backbone can be altered, and consequently the position and pose of the robot's tip can vary in a certain range. Nitinol is widely used in these robots due to its outstanding elasticity [12]. Figure 1 shows a concentric-tube robot consisting of three tubes.

3 Equivalent Conservative System for Concentric-Tube Robots Subject to External Forces

The widely used geometrically exact model always involves the complex force analysis of tubes. To simplify the model, this paper propose an alternative conservative system: a robot with an object hanging at its tip, as shown in Fig. 2; the weight of the object is the value of the external force $\boldsymbol{F}$, and the direction of gravity is the direction of the external force. Since the weights of the tubes are neglected,

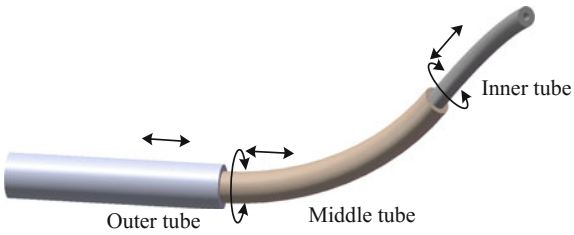

Fig. 1 A concentric-tube robot consisting of three tubes

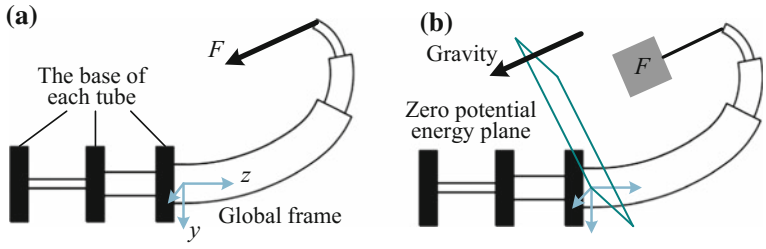

Fig. 2 The equivalent conservative system for the concentric-tube robot subject to an external force. The external force is replaced with an object hanging at the robot's tip

the potential energy of this alternative system only includes the elastic energy of each tube and the gravitational potential energy of the object. Note that the zero potential energy plane passes through the origin of the global frame and it is perpendicular to the external force $\boldsymbol{F}$.

4 Kinematic Model of Concentric-Tube Robots

4.1 Modeling Assumptions

Since all component tubes in the robot are long and thin, the basic assumptions of the Kirchhoff-rod theory are adopted in this paper: (1) the extension and transverse shear deformation of the tubes are neglected; (2) the linear constitutive equations for both bending and torsion are adopted.

In addition, for clarity in deriving the fundamental equations, the weights of tubes and friction between them are neglected. The tubes are considered to be strictly concentric. Experiments show that these aspects have little influence on the equilibrium conformation model [5, 10], and most of the prior models adopt these assumptions.

4.2 Geometric Descriptions of a Curving Tube

The undeformed curving backbone of a tube can be described by an arc-length parameterized curve $\boldsymbol{r}^*(s)$. And along this curve, the well-known Bishop frames [5] can be defined. By the convention of the Bishop frames, the z-axes are always in the instantaneous tangential direction of the curve, and the frames will not rotate around their z-axis along the curve. Therefore the Bishop frame is also known as the no-torsion frame. The Bishop frames $\{\mathrm{F}^*(\mathrm{s})\}$ for a undeformed tube can be described in the global frame $\{\mathrm{W}\}$ with a series of transformations $\boldsymbol{g}^*(s)$, which consist of position vectors $\boldsymbol{r}^*(s)$ and rotation matrices $\boldsymbol{R}^*(s)$ as

$$\boldsymbol{g}^*(s)=\begin{bmatrix}\boldsymbol{R}^*(s) & \boldsymbol{r}^*(s)\\ \boldsymbol{0}^{\mathrm{T}} & 1\end{bmatrix} \tag{1}$$

If the arc-length parameter s is replaced with time variable t, this can be considered as the homogeneous transformation description of rigid motion. Then drawing on the rigid motion theory [13], a twist can be defined as

$$\boldsymbol{\xi}^*(s)=\begin{bmatrix}\boldsymbol{v}^{*\mathrm{T}}(s) & \boldsymbol{\omega}^{*\mathrm{T}}(s)\end{bmatrix}^{\mathrm{T}}=\left(\boldsymbol{g}^{*-1}(s)\dot{\boldsymbol{g}}^*(s)\right)^{\vee} \tag{2}$$

where $\boldsymbol{v}^*(s) = \boldsymbol{e}_3 = [0\ 0\ 1]^{\mathrm{T}}$ in this case, and $\boldsymbol{\omega}^*(s)$, implying the curvature of the rod (similar to the angular velocity of a rotation), is defined as the curvature vector in the local frame. In this paper, the dot over the variable represents the derivative of the variable with respect to arc-length s. The operator $\mathbf{v}$ represents the transformation $\mathrm{R}^{4\times4}$ (or $\mathrm{R}^{3\times3}$) to R^6 (or R^3), given by the following equation

$$\begin{pmatrix} 0 & -a_3 & a_2 & b_1 \\ a_3 & 0 & -a_1 & b_2 \\ -a_2 & a_1 & 0 & b_3 \\ 0 & 0 & 0 & 0 \end{pmatrix}^{\vee} = (\,a_1 \quad a_2 \quad a_3 \quad b_1 \quad b_3 \quad b_3\,)^T \tag{3}$$

Also, the inverse operation is denoted by $^{\wedge}$. The detailed discussion on the related notations can be found in [13]. The relationship between $\boldsymbol{\omega}^*(s)$ and $\boldsymbol{R}^*(s)$ is as follows:

$$\boldsymbol{\omega}^*(s) = \left(\boldsymbol{R}^{*\mathrm{T}}(s)\dot{\boldsymbol{R}}^*(s)\right)^{\vee} \tag{4}$$

The deformation of a pre-curved tube from its initial state to a new state corresponds to a variation of frames from $\{\mathrm{F}^*(s)\}$ to $\{\mathrm{F}(s)\}$, also corresponds to a variation from $\boldsymbol{g}^*(s)$ to $\boldsymbol{g}(s)$, and a variation from $\boldsymbol{\xi}^*(s)$ to $\boldsymbol{\xi}(s)$ (denoted by $\Delta\boldsymbol{\xi}(s)$). The new frames $\{\mathrm{F}(s)\}$ do not necessarily abide by the convention of the Bishop frames.

4.3 Kinematic Equations of Concentric-Tube Robots

The inputs of the concentric-tube robot are the translation and rotation of each component tube at the corresponding base. Let $s = a_i$ and $\theta_i(a_i)$ denote the translation and rotation inputs of the ith tube, also let $s = b_i$ denotes the arc-length location of the ith tube's tip, where i identifies the tubes from outer to inner. The shape of the concentric-tube robot can also be described by the Bishop frames $\{\mathrm{B}(s)\}$ along with other variables. The Bishop frame at the arc-length location $s = 0$, is set as the global frame $\{\mathrm{W}\}$. According to Sect. 3.2, $\{\mathrm{B}(s)\}$ can also be described in the global frame $\{\mathrm{W}\}$ with position vectors $\boldsymbol{r}(s)$ and rotation matrices $\boldsymbol{R}(s)$, which satisfy

$$\dot{\boldsymbol{r}}(s) = \boldsymbol{R}(s)\boldsymbol{e}_3 \tag{5}$$

$$\dot{\boldsymbol{R}}(s) = \boldsymbol{R}(s)\left((\,\omega_x \quad \omega_y \quad 0\,)^T\right)^{\wedge} \tag{6}$$

where $(\omega_x, \omega_y, 0)^{\mathrm{T}}$ is the curvature vector of $\{\mathrm{B}(s)\}$. Since the tubes are assembled concentrically, the x-y components of each tube's curvature vector in the equilibrium conformation are equivalent respectively if they are expressed in a common

frame. When they are expressed in the robot's Bishop frames, they all equals $(\omega_x, \omega_y)^{\mathrm{T}}$, which is denoted by $\boldsymbol{\omega}_{xy}(s)$. The frames $\{\mathrm{F}_i(\mathrm{s})\}$ for each tube differ from the robot's Bishop frames $\{\mathrm{B}(\mathrm{s})\}$ by a rotation around the local z-axes; that is

$$\boldsymbol{R}_i(s) = \boldsymbol{R}(s)\boldsymbol{R}_z(\theta_i(s)) = \boldsymbol{R}\begin{bmatrix} \cos\theta_i(s) & \sin\theta_i(s) & 0 \\ \sin\theta_i(s) & \cos\theta_i(s) & 0 \\ 0 & 0 & 1 \end{bmatrix} \tag{7}$$

where $\boldsymbol{R}(s)$ and $\boldsymbol{R}_i(s)$ are rotation matrices of $\{\mathrm{B}(\mathrm{s})\}$ and $\{\mathrm{F}_i(\mathrm{s})\}$ with respect to $\{\mathrm{W}\}$, $\theta_i(s)$ is the rotation angle from x-axes of $\{\mathrm{B}(\mathrm{s})\}$ to x-axes of $\{\mathrm{F}_i(\mathrm{s})\}$, and $\theta_i(a_i)$ is the aforementioned input angle of the ith tube at its base. Figure 3 shows the relationship of $\{\mathrm{F}_i^*(\mathrm{s})\}$, $\{\mathrm{F}_i(\mathrm{s})\}$ and $\{\mathrm{B}(\mathrm{s})\}$.

Based on the above analysis, the x-y components of the ith tube's curvature vector can be expressed as

$$\boldsymbol{\omega}_{i,xy}(s) = \boldsymbol{R}_z(\theta_i(s))|_{xy}^T \boldsymbol{\omega}_{xy}(s) \tag{8}$$

where

$$\boldsymbol{R}_z(\theta_i(s))|_{xy} = \begin{pmatrix} \cos\theta_i(s) & -\sin\theta_i(s) \\ \sin\theta_i(s) & \cos\theta_i(s) \end{pmatrix} \tag{9}$$

$$\boldsymbol{\omega}_{i,xy}(s) = \begin{pmatrix} \omega_{i,x}(s) & \omega_{i,y}(s) \end{pmatrix}^T \in R^2 \tag{10}$$

Besides, according to Eqs. (4) and (7), the third component of the ith tube's curvature vector $(\omega_{i,z}(s))$ is equal to $\dot{\theta}_i(s)$. Define $\boldsymbol{\theta}(s) = (\theta_1,\ \theta_2,\ \theta_3)^{\mathrm{T}}$, and $\boldsymbol{\omega}_z(s) = (\omega_{1,z},\ \omega_{2,z},\ \omega_{3,z})^{\mathrm{T}}$, then we have

$$\dot{\boldsymbol{\theta}}(s) = \boldsymbol{\omega}_z(s) \tag{11}$$

The model of the concentric-tube robot should also include the linear constitutive relationship of Nitinol, which can be described in potential energy form as

$$E_i(s) = \int \frac{1}{2}\left(\boldsymbol{\omega}_i - \boldsymbol{\omega}_i^*\right)^T \boldsymbol{K}_i(s)\left(\boldsymbol{\omega}_i - \boldsymbol{\omega}_i^*\right)\mathrm{d}s \tag{12}$$

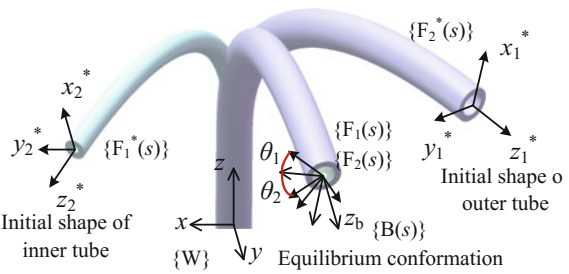

Fig. 3 The tubes' initial states and equilibrium states. In the equilibrium conformation, both tubes are bended and twisted

where $\boldsymbol{\omega}_i^*$ and $\boldsymbol{\omega}_i$ are the curvature vectors of the initial shape and the deformed shape respectively, and stiffness matrix $\boldsymbol{K}_i(s)$ can be expressed as

$$\boldsymbol{K}_i(s)=\begin{bmatrix} K_{i,xy}(s) & 0 & 0 \\ 0 & K_{i,xy}(s) & 0 \\ 0 & 0 & K_{i,z}(s) \end{bmatrix} \tag{13}$$

and $K_{i,xy}(s)$ is the bending stiffness of the ith tube in its x and y directions, and $K_{i,z}(s)$ is the torsional stiffness of the ith tube.

Normally, the lengths of the tubes in a robot are not equal. The outer tube is the shortest while the inner tube is the longest. For convenience, virtual tubes are added to the tips and the bases of the outer and the middle tubes, so that the tubes are fully overlapped over $[a_3, b_3]$. The virtual tubes at the bases are designated with infinite bending and torsional rigidity, and the virtual tubes at the tips are designated with zero bending and torsional rigidity. In this way, this fully overlapped model is equivalent to the original model.

5 Equilibrium Conformation of Concentric-Tube Robots

The static equilibrium configuration of a conservative system should conform to the minimum potential energy principle, which states that the total potential energy function is stationary at the static equilibrium configuration [11]. Therefore, the first variation of the potential energy function at the static equilibrium configuration should be zero. This problem can be solved utilizing the optimal control theory. According to the aforementioned alternative system, the total potential energy function is as follows:

$$J = -\boldsymbol{F}^T\boldsymbol{r}(b_3) + \int_{a_3}^{b_3} \sum_{i=1}^{3} \frac{1}{2}\left(\boldsymbol{\omega}_i - \boldsymbol{\omega}_i^*\right)^T \boldsymbol{K}_i(s)\left(\boldsymbol{\omega}_i - \boldsymbol{\omega}_i^*\right)\mathrm{d}s \tag{14}$$

The first part of the function J represents the gravitational potential energy of the object, and the integral term represents the bending and torsional energy along the arc-length of all tubes. Substituting (8) into (14) can eliminate $\boldsymbol{\omega}_i$ in the potential energy, and yields

$$J = -\boldsymbol{F}^T\boldsymbol{r}(b_3) + \int_{a_3}^{b_3} \frac{1}{2}\sum_{i=1}^{3} \left(K_{i,z}\left(\dot{\theta}_i - \omega_{i,z}^*\right)^2 + K_{i,xy}\left|\boldsymbol{R}_z(\theta_i)\right|_{xy}^T \boldsymbol{\omega}_{xy} - \boldsymbol{\omega}_{i,xy}^*\right|^2 \Big)\mathrm{d}s \tag{15}$$

where symbol $|\cdot|$ denotes the module of the vector, $\boldsymbol{\omega}_{i,xy}^{*} \in \mathrm{R}^2$ is the x-y components of $\boldsymbol{\omega}_i^{*}$, $\omega_{i,z}^{*} \in \mathrm{R}$ is the third component of $\boldsymbol{\omega}_i^{*}$. For convenience, the term of gravitational potential energy is denoted by $\varphi(\boldsymbol{r})$, and the integrand term is denoted by Lagrangian function L.

The function J can be interpreted as the cost function of a control system with arc-length parameter s interpreted as time parameter t. Then we have its state vector and control vector as follows

$$\boldsymbol{x}(s)=(\boldsymbol{r}(s),\boldsymbol{R}(s),\boldsymbol{\theta}(s)) \in R^3 \times R^{3\times 3} \times R^3 \tag{16}$$

$$\boldsymbol{u}(s)=\left(\boldsymbol{\omega}_{xy}(s),\boldsymbol{\omega}_z(s)\right) \in R^2 \times R^3 \tag{17}$$

and its state equations as (5), (6) and (11).

Therefore, drawing on the optimal control theory [14], the Hamiltonian function can be defined as:

$$\begin{aligned} H(\boldsymbol{x},\boldsymbol{u},\boldsymbol{\lambda},s) = {} & \frac{1}{2}\sum_{i=1}^{n}\left(K_{i,z}\left(\omega_{i,z}-\omega_{i,z}^{*}\right)^2\right) \\ & + \frac{1}{2}\sum_{i=1}^{n}\left(K_{i,xy}\left|\boldsymbol{R}_z(\theta_i)\big|_{xy}^{T}\boldsymbol{\omega}_{xy}-\boldsymbol{\omega}_{i,xy}^{*}\right|^2\right) + \boldsymbol{\lambda}_{\boldsymbol{r}}^{T}\boldsymbol{R}\boldsymbol{e}_z + \mathrm{tr}\left(\boldsymbol{\lambda}_{\boldsymbol{R}}^{T}\boldsymbol{R}\begin{bmatrix}\omega_x\\ \omega_y\\ 0\end{bmatrix}^{\wedge}\right) + \boldsymbol{\lambda}_{\theta}^{T}\boldsymbol{\omega}_z \end{aligned} \tag{18}$$

where $\boldsymbol{\lambda} = (\boldsymbol{\lambda}_{\boldsymbol{r}}^{\mathrm{T}}, \boldsymbol{\lambda}_{\boldsymbol{R}}^{\mathrm{T}}, \boldsymbol{\lambda}_{\boldsymbol{\theta}}^{\mathrm{T}})^{\mathrm{T}} \in \mathrm{R}^3 \times \mathrm{R}^{3\times 3} \times \mathrm{R}^3$ is the Lagrange multiplier. The component multipliers $\boldsymbol{\lambda}_{\boldsymbol{r}}^{\mathrm{T}}$, $\boldsymbol{\lambda}_{\boldsymbol{R}}^{\mathrm{T}}$, $\boldsymbol{\lambda}_{\boldsymbol{\theta}}^{\mathrm{T}}$ can be considered as the generalized forces on the generalized coordinates $\boldsymbol{r}$, $\boldsymbol{R}$ and $\boldsymbol{\theta}$ respectively.

Obviously, this optimal control problem has the Bolza-type cost function, and it is under no terminal constraints. According to the fundamental optimal control theory [14], the first order necessary conditions for stationarity along entire trajectory include the canonical equations, the extreme conditions and the boundary conditions, as follows:

$$\begin{cases} \dot{\boldsymbol{\lambda}}_{\boldsymbol{r}} = -\frac{\partial H}{\partial \boldsymbol{r}} = (0 \quad 0 \quad 0), \dot{\boldsymbol{\lambda}}_{\boldsymbol{R}} = -\frac{\partial H}{\partial \boldsymbol{R}} = -\boldsymbol{e}_z\boldsymbol{\lambda}_{\boldsymbol{r}}^{T} - \begin{bmatrix}\omega_x\\ \omega_y\\ 0\end{bmatrix}^{\wedge}\boldsymbol{\lambda}_{\boldsymbol{R}}^{T}, \\ \dot{\boldsymbol{\lambda}}_{\boldsymbol{\theta}} = -\frac{\partial H}{\partial \boldsymbol{\theta}} = \begin{pmatrix} K_{1,xy}\boldsymbol{\omega}_{1,xy}^{*\,T} & \boldsymbol{R}_{d,1}\boldsymbol{\omega}_{xy} \\ K_{2,xy}\boldsymbol{\omega}_{2,xy}^{*\,T} & \boldsymbol{R}_{d,2}\boldsymbol{\omega}_{xy} \\ K_{3,xy}\boldsymbol{\omega}_{3,xy}^{*\,T} & \boldsymbol{R}_{d,3}\boldsymbol{\omega}_{xy}^{T} \end{pmatrix}^{T} \end{cases} \tag{19}$$

$$\begin{cases} \frac{\partial H}{\partial \boldsymbol{\omega}_{xy}} = \sum_{i=1}^{n} K_{i,xy}\left(\boldsymbol{\omega}_{xy} - \boldsymbol{R}_z(\theta_i)\boldsymbol{\omega}^*_{i,xy}\right)^T + \begin{pmatrix} \left(\boldsymbol{\lambda}_{\boldsymbol{R}}^T\boldsymbol{R}\right)_{23} - \left(\boldsymbol{\lambda}_{\boldsymbol{R}}^T\boldsymbol{R}\right)_{32} \\ -\left(\boldsymbol{\lambda}_{\boldsymbol{R}}^T\boldsymbol{R}\right)_{13} + \left(\boldsymbol{\lambda}_{\boldsymbol{R}}^T\boldsymbol{R}\right)_{31} \end{pmatrix}^T = 0, \\ \frac{\partial H}{\partial \omega_z} = \begin{pmatrix} K_{1,z}\left(\omega_{1,z} - \omega^*_{1,z}\right) \\ K_{2,z}\left(\omega_{2,z} - \omega^*_{2,z}\right) \\ K_{3,z}\left(\omega_{3,z} - \omega^*_{3,z}\right) \end{pmatrix}^T + \boldsymbol{\lambda}_\theta^T = 0 \end{cases} \tag{20}$$

$$\begin{cases} \boldsymbol{r}(a_3) = (\,0 \quad 0 \quad a_3\,)^T, \boldsymbol{R}(a_3) = \boldsymbol{I}, \boldsymbol{\theta}(a_3) = \boldsymbol{\theta}_{\text{base}}, \\ \boldsymbol{\lambda}_{\boldsymbol{r}}(b_3) = \frac{\partial \varphi}{\partial \boldsymbol{r}(b_3)} = -\boldsymbol{F}, \boldsymbol{\lambda}_{\boldsymbol{R}}(b_3) = \frac{\partial \varphi}{\partial \boldsymbol{R}(b_3)} = 0, \boldsymbol{\lambda}_{\boldsymbol{\theta}}(b_3) = \frac{\partial \varphi}{\partial \boldsymbol{\theta}(b_3)} = 0 \end{cases} \tag{21}$$

where

$$\boldsymbol{R}_{d,i} = \begin{bmatrix} -\sin\theta_i & \cos\theta_i \\ -\cos\theta_i & -\sin\theta_i \end{bmatrix} \tag{22}$$

$(\boldsymbol{A})_{ij}$ denotes the ith row and jth Column element of matrix $\boldsymbol{A}$, $\boldsymbol{I}$ denotes the 3×3 identical matrix, $\boldsymbol{\theta}_{\text{base}} = \{\theta_1(a_3), \theta_2(a_3), \theta_3(a_3)\}^{\text{T}}$ is a column vector consists of the rotation angles of all tubes at the base.

In the above discussion, the admissible trajectories for the optimal control problem are assumed to be continuous and to have continuous first derivatives; that is, the trajectories are smooth. However, for concentric-tube robots, the trajectories are usually discontinuous at several discrete points owing to the following facts: (1) the precurvature of each tube is usually piecewise-constant along the full arc-length; e.g., a typical tube comprising a straight portion and a constant curvature portion; (2) owing to the aforementioned virtual tubes, the bending stiffness and torsional stiffness are also piecewise-constant along the full arc-length. These two kinds of points are shown in Fig. 4. They are both referred to as corner points.

Therefore, the admissible trajectories should satisfy the additional necessary conditions, as follows [14]:

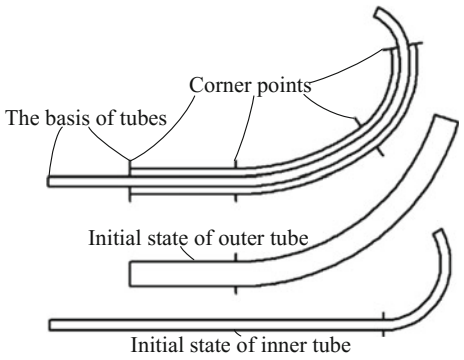

Fig. 4 The corner points in a robot. The two corner points in the middle are emerged because of the pre-curvature mutation of the tubes. The first and the last corner points are emerged since the tubes are not fully overlapped

$$\begin{cases} \frac{\partial L}{\partial \dot{\boldsymbol{x}}}\big|_{s_j^-} = \frac{\partial L}{\partial \dot{\boldsymbol{x}}}\big|_{s_j^+} \\ \left(L - \dot{\boldsymbol{x}}^T \frac{\partial L}{\partial \dot{\boldsymbol{x}}}\right)\big|_{s_j^-} = \left(L - \dot{\boldsymbol{x}}^T \frac{\partial L}{\partial \dot{\boldsymbol{x}}}\right)\big|_{s_j^+} \end{cases} \tag{23}$$

where j is the number of the corner points, s_j is the arc-length location of corner point j. They are determined by the inputs of each tube.

In conclusion, the equilibrium conformation model of the robot comprises the differential Eqs. (19)–(20), boundary conditions (21) and corner point conditions (23) with respect to shape parameter set $\{\boldsymbol{r}(s), \boldsymbol{R}(s), \boldsymbol{\theta}(s)\}$. Normally, this various point boundary value problem (BVP) cannot be solved analytically. The common numerical methods for it include shooting method and difference method [15]. For a number of inputs, several corresponding configurations may emerge [16, 17]. The robot will take the configuration which is near its last configuration. Therefore we can take the parameters of its last configuration as the initial guess for the shooting processes. In addition, the stability of the configurations can be assessed utilizing methods in Ref. [17] in order to avoid snapping.

6 Numerical Examples

In this section, an intuitional two-tube robot is selected to demonstrate the effects of the external forces on the robot. Each tube's initial backbone shape is a section of a circle, and they are fully overlapped during the simulation. The processes of solving differential equations are implemented in Matlab using shooting method. It is assumed that both tubes not only have the same initial backbone shape and arc-length, but also have the same bending stiffness ($K_{i,xy}$) and torsional stiffness ($K_{i,z}$). The values of related parameters are listed in Table 1.

Figure 5 shows the equilibrium conformation under different loads when the outer and inner tubes were rotated to angles of −30° and 30° respectively. The unloaded equilibrium conformation lies on yz-plane, which agrees with the instinct. When the external force is applied to the robot's tip in y-direction, the updated equilibrium conformation still lies on yz-plane, as Fig. 5 shows. This is similar to the bending of a single cantilevered rod. Under the tip force of 5 N, the robot's tip is deflected from its initial position by about 30 mm.

Table 1 Parameters of the robot

Parameters	Values
Total arc-length (mm)	84
Pre-curvature (mm^{-1})	1/60
Curvature vector of the tubes' initial shape	(1/60, 0, 0)
Bending stiffness (Nm^2)	0.0202
Torsional stiffness (Nm^2)	0.0156

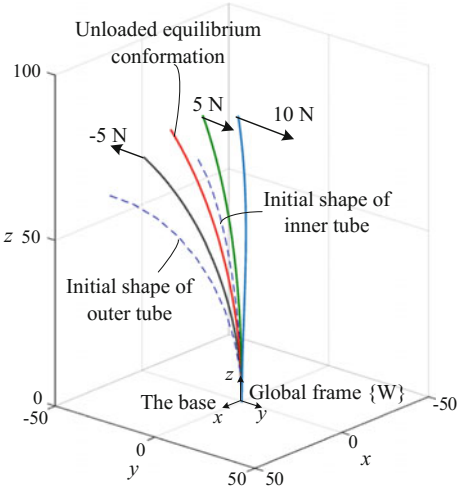

Fig. 5 The equilibrium conformation of the robot subject to different tip loads

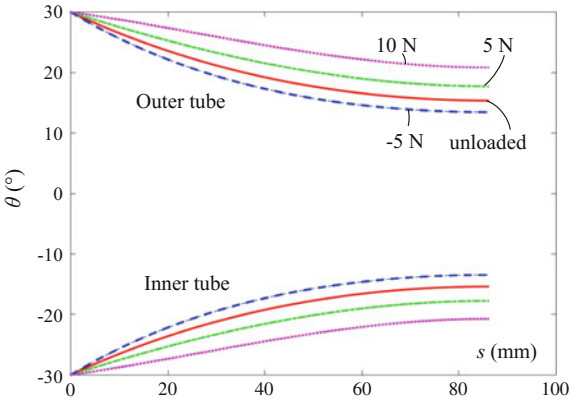

Fig. 6 The rotation angles of both tubes along the whole arc-length for the robot under y-direction tip forces

The rotation angles $\theta_1(s)$ and $\theta_2(s)$ of both tubes, which cannot be observed from the conformation figure, are also changed under loads. Figure 6 shows how the rotation angles vary along the whole arc-length in the loaded robot. At the common base of both tubes, the rotation angles of them are input angles. From the base to the tip, the outer tube twist about the local $-z$-axes, while the inner tube twist about the local z-axes; therefore, the angle between $\{F_1(s)\}$ and $\{F_2(s)\}$ is decreasing. Also, the tip force in the $+y$-direction, which tend to "straighten" the robot, will slowdown this trend, while the tip force in the $-y$-direction will accelerate this trend.

If this robot is under $+x$-direction tip forces, the rotation angles of both tubes along the whole arc-length are shown in Fig. 7. The rotation angles of both tubes are no longer symmetrical with respect to the line $\theta(s) = 0$. The load accelerates the increasing trend of the inner tube's rotation angle, and slowdowns even reverses the decreasing trend of the outer tube's rotation angle. Furthermore, In contrast with y-

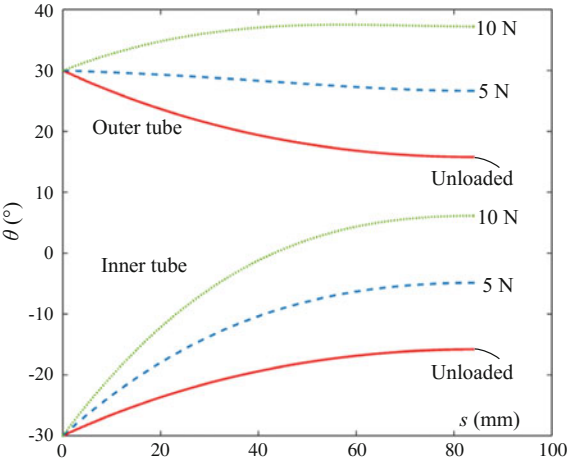

Fig. 7 The rotation angles of both tubes along the whole arc-length for the robot under *x*-direction tip forces

direction tip forces, the effects of *x*-direction tip forces on the rotation angles are much larger, since the torque generated by *x*-direction tip forces are much larger.

7 Conclusions

This paper proposes an equivalent conservative system for the concentric-tube robot under loads, and utilizes the minimum potential energy principle and the optimal control theory to derive the equations of equilibrium conformation. Through numerical simulation, the effects of external forces on the robot's tip are analyzed, and the results show that the externally loaded concentric-tube robot will bend like a single cantilevered rod. The tip forces which tend to "straighten" the robot (i.e. in the +y-direction) will slightly exaggerate the angle between the tubes' local frames at the tip, while the forces in the *x*-direction will affect the rotation angles of both tubes significantly. This model will facilitate the motion planning of the concentric-tube robot while it is performing an interactive task.

Acknowledgments The authors acknowledge the support from the National Natural Science Foundation of China (51175013).

References

1. Webster III RJ, Okamura AM, Cowan NJ (2006) Toward active cannulas: miniature snake-like surgical robots. In: IEEE/rsj international conference on intelligent robots and systems. IEEE Press, New York, pp 2857–2863

2. Sears P, Dupont P (2006) A steerable needle technology using curved concentric tubes. In: IEEE/rsj international conference on intelligent robots and systems. IEEE Press, New York, pp 2850–2856
3. Furusho J (2010) Curved multi-tube systems for fetal blood sampling and treatments of organs like brain and breast. J Comput Assist Radiol Surg 6:223–226
4. Rucker DC, Croom JM, Webster RJ III (2009) Aiming surgical lasers with an active cannula. ASME J Med Devices 3:027506–027510
5. Webster RJ III, Romano JM, Cowan NJ (2009) Mechanics of pre-curved-tube continuum robots. IEEE Trans Robot 25:67–78
6. Burgner J, Swaney PJ, Bruns TL, Clark MS, Rucker DC, Burdette EC (2012) An autoclavable steerable cannula manual deployment device: design and accuracy analysis. ASME J Med Devices 6:410071–410077
7. Swaney PJ, Croom JM, Burgner J, Gilbert HB, Rucker DC, Webster III RJ (2012) Design of a quadra manual robot for single-nostril skull base surgery. In: 2012 ASME dynamic systems and control conference. ASME Press, New York, pp 387–393
8. Trivedi D, Lotfi A, Rahn CD (2008) Geometrically exact models for soft robotic manipulators. IEEE Trans Robot 24:773–780
9. Xu K, Simaan N (2008) An investigation of the intrinsic force sensing capabilities of continuum robots. IEEE Trans Robot 24:576–587
10. Rucker DC, Jones BA, Webster RJ III (2010) A geometrically exact model for externally loaded concentric-tube continuum robots. IEEE Trans Robot 26:769–780
11. Antman SS (1976) Nonlinear problems of elasticity. Springer, Berlin
12. Berg BT (1995) Bending of superelastic wires, part I: experimental aspects. ASME J Appl Mech 62
13. Murray RM, Sastry SS, Li Z (1994) A mathematical introduction to robotic manipulation. CRC Press, Boca Raton
14. Bryson AE, Ho YC, Siouris GM (1975) Applied optimal control: optimization, estimation, and control. Halsted Press, New York
15. Kincaid D, Cheney W (1991) Numerical analysis: mathematics of scientific computing. Brooks/Cole Publishing Co., New York
16. Ha J, Park FC, Dupont PE (2015) Elastic stability of concentric tube robots subject to external loads. IEEE Trans Biomed Eng 26:1–13
17. Gilbert HB, Hendrick RJ, Webster RJ III (2015) Elastic stability of concentric tube robots: a stability measure and design test. IEEE Trans Robot 32:1–16